POLITECNICO DI TORINO
Repository ISTITUZIONALE

High-resolution high-accuracy orthophoto map and digital surface model of Forni Glacier tongue (Central Italian Alps) from UAV photogrammetry

Original
High-resolution high-accuracy orthophoto map and digital surface model of Forni Glacier tongue (Central Italian Alps) from UAV photogrammetry / Belloni, V., Di Rita, M., Fugazza, D., Traversa, G., Hanson, K., Diolaiuti, G., Crespi, M.. - In: JOURNAL OF MAPS. - ISSN 1744-5647. - 19:1(2023). [10.1080/17445647.2023.2217508]

Availability:
This version is available at: 11583/2990317 since: 2024-07-03T13:18:56Z

Publisher:
Taylor and Francis Ltd.

Published
DOI:10.1080/17445647.2023.2217508

Terms of use:

This article is made available under terms and conditions as specified in the corresponding bibliographic description in the repository

Publisher copyright

(Article begins on next page)

08 September 2026

Journal of Maps

ISSN: (Print) (Online) Journal homepage: www.tandfonline.com/journals/tjom20

High-resolution high-accuracy orthophoto map and digital surface model of Forni Glacier tongue (Central Italian Alps) from UAV photogrammetry

Valeria Belloni, Martina Di Rita, Davide Fugazza, Giacomo Traversa, Kevin Hanson, Guglielmina Diolaiuti & Mattia Crespi

To cite this article: Valeria Belloni, Martina Di Rita, Davide Fugazza, Giacomo Traversa, Kevin Hanson, Guglielmina Diolaiuti & Mattia Crespi (2023) High-resolution high-accuracy orthophoto map and digital surface model of Forni Glacier tongue (Central Italian Alps) from UAV photogrammetry, Journal of Maps, 19:1, 2217508, DOI: 10.1080/17445647.2023.2217508

To link to this article: https://doi.org/10.1080/17445647.2023.2217508

© 2023 The Author(s). Published by Informa UK Limited, trading as Taylor & Francis Group on behalf of Journal of Maps

View supplementary material

Published online: 24 Jun 2023.

Submit your article to this journal

Article views: 1290

View related articles

View Crossmark data

Citing articles: 1 View citing articles

Full Terms & Conditions of access and use can be found at
https://www.tandfonline.com/action/journalInformation?journalCode=tjom20

JOURNAL OF MAPS
2023, VOL. 19, NO. 1, 2217508
https://doi.org/10.1080/17445647.2023.2217508

SCIENCE

OPEN ACCESS Check for updates

High-resolution high-accuracy orthophoto map and digital surface model of Forni Glacier tongue (Central Italian Alps) from UAV photogrammetry

Valeria Belloni [a], Martina Di Rita [b], Davide Fugazza [c], Giacomo Traversa [d], Kevin Hanson[b], Guglielmina Diolaiuti [c] and Mattia Crespi [a,e]

[a]Geodesy and Geomatics Division, DICEA, Sapienza University of Rome, Rome, Italy; [b]Leica Geosystems AG, Heerbrugg, Switzerland; [c]Department of Environmental Science and Policy, University of Milan, Milan, Italy; [d]ISP-CNR, Milan, Italy; [e]Sapienza School for Advanced Studies, Sapienza University of Rome, Rome, Italy

ABSTRACT

This work presents the high-resolution high-accuracy orthophoto map and the Digital Surface Model of Forni Glacier (Italian Alps). These represent the status of the glacier tongue in mid-August 2022 when surveys were carried out with a DJI Phantom 4 RTK drone. The processing was carried out in Leica Infinity, and a 3 cm orthomosaic and a 20 cm Digital Surface Model were generated and made available for analysis of the current status of the glacier, which shows signs of downwasting, with the occurrence of collapsing areas and a rapidly changing proglacial landscape. This work can also be used as a reference to investigate the glacier evolution, also in light of climate change. Accuracy requirements of the deliverables were ensured by combining Post Processed Kinematic and Structure from Motion integrated with bundle block adjustment, and using Ground Control Points and Check Points, to guarantee redundancy and evaluate the geolocation accuracy and precision.

ARTICLE HISTORY
Received 16 January 2023
Revised 5 May 2023
Accepted 17 May 2023

KEYWORDS
high-resolution orthophoto map; digital surface model; Forni Glacier; UAV photogrammetry; accuracy and precision assessment

1. Introduction

In the current global warming phase, mountain glaciers are retreating and losing mass at an unprecedented rate. Over 2017–2019, the mass balance of reference glaciers monitored by the World Glacier Monitoring Service was −1 m w.e., more negative than any other year since observations began (WGMS, 2021), and it is estimated that mountain glaciers contributed 27 mm to sea level rise between 1961 and 2016 (Zemp et al., 2019), with global glacier mass losses exceeding 1 mm per year contribution to sea level rise in 2016–2020 (WGMS, 2021). In the European Alps, glaciers have been retreating at rates of 1.2% per year over the past decade, as revealed by comparing recent inventories based on satellite data (Paul et al., 2020). Glacier mass losses and retreat are synchronous with dramatic changes in the glacier landscape, with increasingly frequent collapses at the glacier terminus (Egli et al., 2021), widening of medial moraines and supraglacial debris cover (Azzoni et al., 2018), and darkening phenomena of biotic and abiotic origin (Di Mauro & Fugazza, 2022).

In the last decades, remote sensing techniques have been widely adopted for generating Digital Surface Models (DSMs) in glacial environments, since DSMs can be used to identify glacier thickness and volume changes and to detect steep areas that are most prone to morphodynamic changes (Blasone et al., 2015; Fugazza et al., 2018). Among remote sensing platforms, Synthetic Aperture Radar (SAR) and optical satellites allow for large-scale monitoring of glaciers and do not suffer from logistic constraints. However, their resolution is limited and they suffer from specific problems related to phase unwrapping and the presence of clouds. On the other hand, Unmanned Aerial Vehicles (UAVs) enable the collection of high spatial resolution data over wide and not accessible areas at a relatively low cost and in an efficient and flexible way. Also, the availability of state-of-the-art software allows for the generation of high-accuracy and high-resolution DSMs, crucial for glacier monitoring. The only drawback of UAVs compared to satellite and aerial surveys is the limitation in area coverage. However, UAVs are usually a suitable tool to focus on the glacier tongue, which is the area subject to the largest changes.

UAV data processing is usually carried out through the Structure from Motion (SfM) technique that traditionally relies on Ground Control Points (GCPs) homogeneously distributed and measured in the study area, to link the image coordinates and the 3D world coordinates (indirect georeferencing) (Maier

CONTACT Davide Fugazza davide.fugazza@unimi.it Department of Environmental Science and Policy, University of Milan, Milan, Italy
Supplemental data for this article can be accessed online at https://doi.org/10.1080/17445647.2023.2217508.
© 2023 The Author(s). Published by Informa UK Limited, trading as Taylor & Francis Group on behalf of Journal of Maps
This is an Open Access article distributed under the terms of the Creative Commons Attribution-NonCommercial License (http://creativecommons.org/licenses/by-nc/4.0/), which permits unrestricted non-commercial use, distribution, and reproduction in any medium, provided the original work is properly cited. The terms on which this article has been published allow the posting of the Accepted Manuscript in a repository by the author(s) or with their consent.

et al., 2022). Following the standard indirect georeferencing approach, Rossini et al. (2018) generated a DSM and an orthophoto map of Morteratsch Glacier (Swiss Alps) with an accuracy (3D RMSE on Check Points – CPs -) of approximately 0.17 m for both models. Similarly, Ioli et al. (2021) generated DSMs of Belvedere Glacier at different epochs from 2015 to 2020, achieving a 3D RMSE between 0.10 and 0.35 m. In previous studies on Forni Glacier, DSMs were generated using an indirect georeferencing approach and a small number of GCPs due to the logistic difficulties in placing the targets; therefore, all the available targets were used as GCPs, reaching a precision of 0.40 m (Fugazza et al., 2018).

Recently, UAVs provided with GNSS Real Time Kinematic (RTK) sensors have largely improved data collection, reducing the need for GCPs since they may directly provide sufficient accuracy for image orientation when GCPs are not available (direct georeferencing). This has the advantage of reducing or even eliminating the need for the placement of GCPs, which is a time-consuming and risky activity, especially in glacier environments. Combining RTK technology and direct georeferencing (Dall'Asta et al., 2017) generated the DSMs of Gran Sometta rock glacier, achieving a 3D RMSE on CPs of 8 cm. However, the RTK connection is not always reliable, especially in the mountain environment where data connection is not always available and there is a high risk of losing the satellite or the radio signal due to occlusions. When RTK is not available, the Post Processing Kinematic (PPK) approach allows for the post-processing of raw GNSS data of UAV using a GNSS reference station placed near the area of interest, achieving the most accurate possible result. In Belloni et al. (2022) a direct georeferencing approach was combined with PPK for compensating RTK signal loss and generating DSMs of a small area of Forni Glacier, achieving a 3D RMSE on CPs of 4 cm.

In this paper we present a high-resolution high-accuracy orthophoto map and a DSM of Forni Glacier (Ortles-Cevedale massif, Italian Alps), generated from a UAV survey carried out in August 2022 by combining the PPK strategy and SfM technique, integrated with bundle block adjustment and usage of ground points, to achieve the best possible result, improving the accuracy of the final deliverables and compensating for common sources of errors in mountain areas. The aims of this work are:

1) To provide up-to-date, highly accurate products for describing the surface morphology of Forni Glacier;
2) To set a reference for future studies, such as glacier retreat computation, ice volume change estimation and morphological evolution, which can help assess the impact of climate change on this glacier and related water resources.

The generation of high-resolution and high-accuracy products makes it possible to characterise in great detail the rapidly changing glacial environments (Rossini et al., 2018) and allows investigating changes at much shorter time scales compared to satellite data.

2. Study area

The study area is Forni Glacier, one of the largest valley glaciers of the Italian Alps (see Figure 1 and Main Map).

The area of Forni Glacier was 10.50 km^2 in 2016 (Paul et al., 2020), with a decrease of 0.84 km^2 from the previous inventory (data from 2007; Smiraglia et al., 2015), i.e. a regression rate of −0.82% per year, in line with the retreat rates of Alpine glaciers. The glacier has three separate accumulation basins, reaching its highest point at S. Matteo peak (3673 m a.s.l.). The basins then join into a single tongue, reaching almost 2500 m a.s.l. at the terminus (Fugazza et al., 2018). In 2015, the eastern tongue became separated from its accumulation basin, while the western part of the tongue is now largely debris covered. The confluence of the ice tongue also marks the origin of two medial moraines, stretching for more than 2 km, whose width has been increasing over the past two decades (Azzoni et al., 2018). Besides medial moraines, the glacier tongue also shows a variety of surface types and morphologies, with increasing debris cover lowering albedo (Fugazza et al., 2016) and evidence of supraglacial streams, moulins and ponds, as well as numerous crevasses and collapses especially occurring at the ice margin (Azzoni et al., 2017; Fugazza et al., 2015) (Figure 2).

Radio Echo sounding measurements carried out in 2012 revealed a maximum ice thickness of 120 m over the western accumulation basin, and an average ice depth of 20–30 m over the glacier tongue (Urbini et al., 2017), whereas the equilibrium line altitude ranges between 2800 and 3200 m a.s.l. (Fugazza et al., 2016). Ice thickness losses have been particularly large since the 2010s, with an average decrease of more than 5 m on the glacier tongue and exceeding 20 m in some areas (Di Rita et al., 2020; Fugazza et al., 2018).

An Automatic Weather Station (AWS) was installed on the eastern part of the glacier tongue in 2005; a second AWS was installed close to it in 2014. In 2015, both AWSs were moved to the central part of the tongue owing to the formation of a circular depression ('ring fault') at their former location (Senese et al., 2018). Based on the first 7 years of data, Senese et al. (2012) described the glacier meteorological surface conditions, finding an average annual air temperature of −1.3°C, with an annual range of

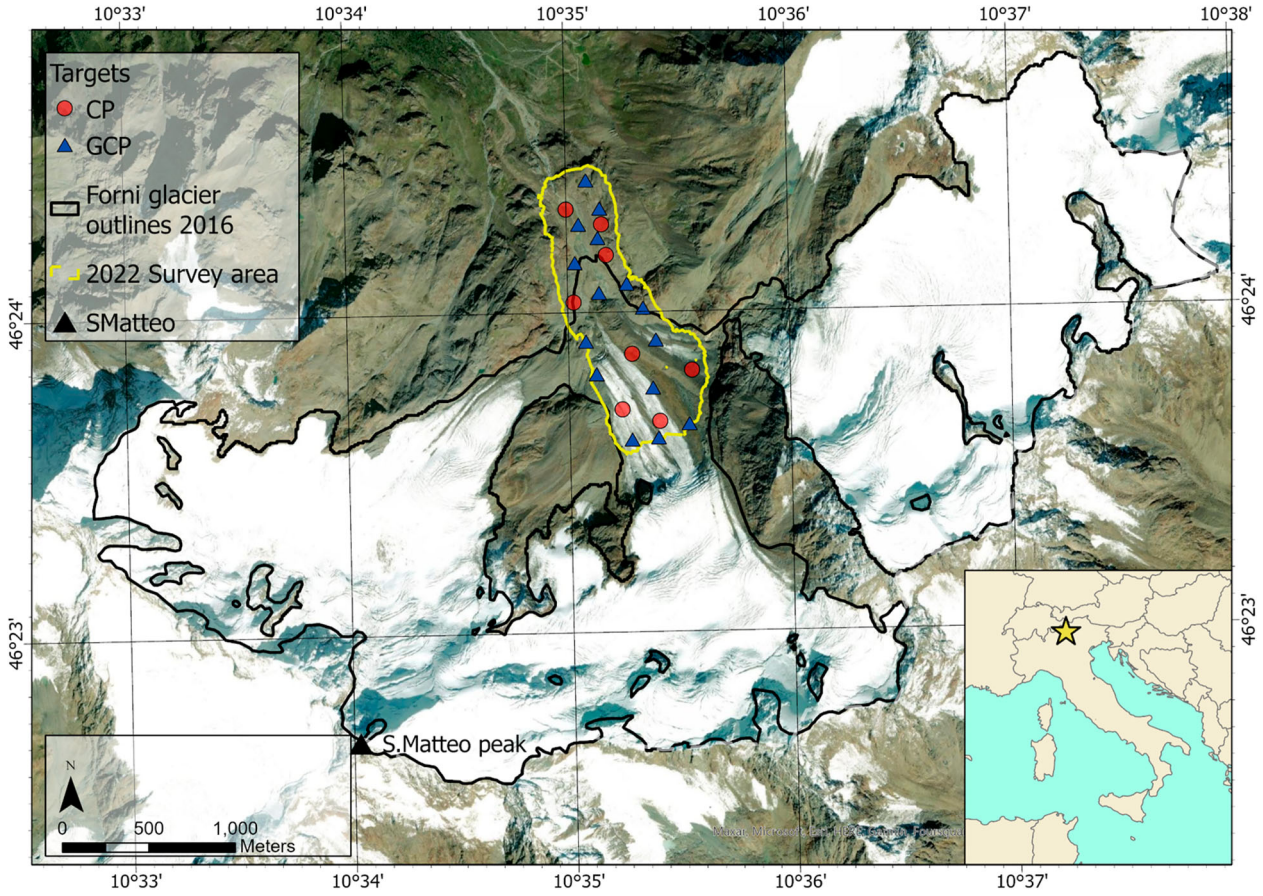

Figure 1. The location of Forni Glacier and study area of the 2022 UAV survey with the positions of the targets.

7.4°C, a mean four-year albedo of 0.65 and mean wind speed of 4.99 ms^{-1}, with a record high of 25.11 ms^{-1}.

In this study, the focus is on the glacier tongue, including its eastern and central parts. The upper limits of the study area include the AWSs in the central sector of the tongue and the entire eastern sector, while downvalley the survey includes the roches moutonnées which were exposed by ice retreat since the 1980s (see Figure 1 and Main Map).

3. Acquisition planning and data collection

The data analysed in this study were acquired during a three-day surveying campaign carried out between the 18th and 20th of August 2022. Careful planning is a crucial step in all surveying tasks, especially when data collection is done in complex areas such as glaciers. Planning for the data collection had to consider the need to establish a local GNSS base station for three aims: (1) store raw GNSS data for computing an accurate position of the base itself, with respect to known permanent stations provided by the Hexagon SmartNet GNSS network; (2) support the intended RTK points measurements over the glacier given the lack of cell coverage; (3) enable the most accurate UAV track kinematic post-processing. Specifically, a Leica GS18 T GNSS receiver was set up close to the Branca hut (situated at 2505 m a.s.l. and 1.5 km far from the glacier terminus) and used as a base, logging raw data and sending real-time corrections to a Leica GS18 I GNSS receiver used as a rover. The rover was used to measure the position of the targets and compute the position of the D-RTK 2 GNSS receiver, used as the base for the UAV.

Before flying the drone, 23 targets were placed in the area of interest on rock outcrops and over the glacier surface (Figure 2), and their positions were measured to be used as ground points for evaluating the precision and accuracy of the geolocation of the overall image block, directly impacting the final accuracy of the DSM and orthophoto map. To ensure the best possible flight plan, the whole area of interest was divided into nine regions and for each of them, a flight was planned (Figure 3).

The shape and the size of each area were identified in Leica Infinity using the DSM generated with the imagery dataset acquired during a previous 2021 campaign (Belloni et al., 2022) and processed with Leica Infinity (Table 1).

In such a way the optimal flight height was defined, making sure to: (1) cover the whole area; (2) obtain a proper Ground Sample Distance (GSD); (3) fly each region with a single battery (avoiding the UAV coming back for a battery change); (4) avoid dangerous situations with the drone being too close to surrounding rock faces. Once created, these areas were

Figure 2. Example of surface characteristics of Forni Glacier: the medial moraine (top left), a collapse at the terminus (top right), supraglacial stream and small moulin with evidence of debris-cover (bottom left), crevasses and debris cover on the glacier tongue (bottom right).

uploaded to the DJI remote controller and to the controller of the GNSS rover, to easily provide an overview of the acquisition area, and obtain guidance for the best places for ground points. Flight parameters were also set during planning: a speed of 4.5 m/s and an average flight height of 70 m above the glacier surface, which resulted in an average GSD of 2.5 cm/pixel. To ensure a constant flight height over the glacier, take-off points at different heights were used. Globally 2101 images were acquired with a 75% lateral and 80% longitudinal overlap over an area of 0.8 km^2.

The flights were performed using a DJI Phantom 4 RTK, equipped with a multi-constellation multi-frequency GNSS receiver and an integrated RTK module. For the RTK navigation, we used a DJI D-RTK 2 GNSS receiver, a high-precision GNSS mobile station connected to the DJI Phantom 4 RTK, that provides real-time differential corrections for generating centimeter-level positioning data and improving absolute accuracy on image metadata, provided the base station is correctly positioned in the used reference frame. During the flights, raw GNSS satellite observations were also automatically stored alongside the images. Figure 4 shows the equipment used during the survey.

4. Data processing

The whole set of data was processed using Leica Infinity, a geospatial surveying software focused on workflows, supporting among others raw GNSS data post-processing and photogrammetric image processing. The software is designed to easily process, combine, and integrate data collected from different kinds of sensors such as GNSS receivers, Terrestrial Laser Scanners, Total Stations, Digital Levels, and Aerial and Terrestrial photogrammetric devices, enabling data processing and visualisation in a common reference frame (Di Rita & Hanson, 2022). From version 3.6.1, released in November 2021, a tool to post-process GNSS kinematic tracks of UAV and automatically update image positions and image position accuracy is also available, along with reporting tools providing transparent information on solution quality (such as fixed or not fixed GNSS solution type, 3D coordinate quality). This tool works with data coming from any drone able to store raw GNSS data and it is dedicated to improving image positioning accuracy and deriving the best possible final deliverables, e.g. Dense Point Clouds (DPCs), DSMs, and orthophoto maps (Belloni et al., 2022).

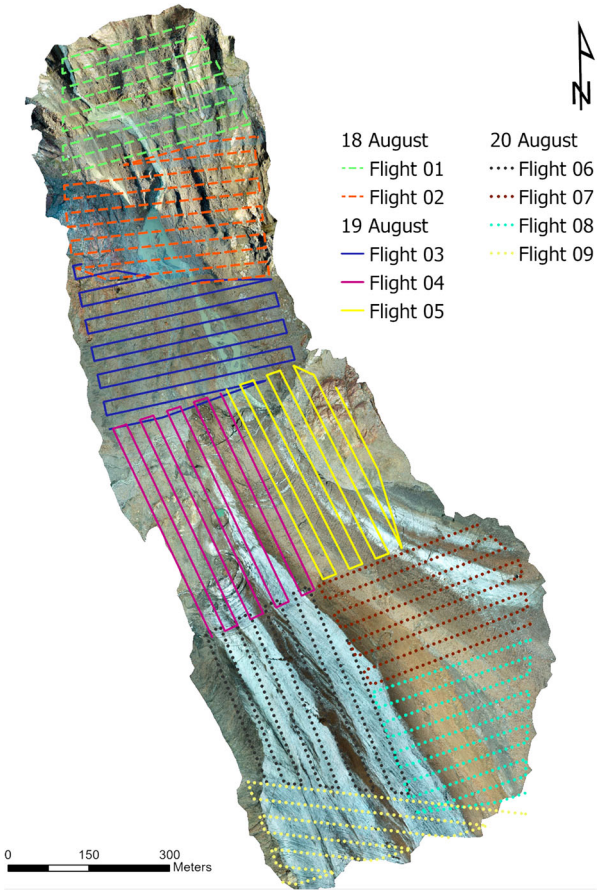

Figure 3. The nine flight lines used in the survey of Forni Glacier.

The first step of data processing was the post-processing of the raw GNSS data of the local base set at the Branca hut, using as reference raw GNSS data acquired by a network of permanent stations (ETRF2000 reference system). For this, HxGN SmartNet service was used and Rinex files from four reference stations around the area of interest were downloaded and imported into Leica Infinity. The selected reference stations and their distances to the Branca hut were Silano (29 km), Tirano (38 km), Bienno (57 km), and Appiano (53 km), as shown in Figure 5.

Once the position of the base at the Branca hut was updated, so were automatically the positions of the targets acquired with the rover connected to the base.

Table 1. Date, area covered and number of images in each of the individual flights of the survey of Forni Glacier.

ID	Date	Area covered	Number of images
Flight 01	18.08.2022	80,000 m^2	225
Flight 02	18.08.2022	95,000 m^2	268
Flight 03	19.08.2022	98,000 m^2	303
Flight 04	19.08.2022	99,000 m^2	300
Flight 05	19.08.2022	80,000 m^2	244
Flight 06	20.08.2022	92,000 m^2	223
Flight 07	20.08.2022	77,000 m^2	148
Flight 08	20.08.2022	80,000 m^2	146
Flight 09	20.08.2022	85,000 m^2	244

The second step consisted of post-processing the GNSS tracks acquired in each flight, using as a reference the updated position of the base at the Branca hut. A dedicated import for images together with GNSS tracks was used. Once the GNSS track was post-processed, image positions were updated; in this way, images and targets were consistently estimated in a common reference frame.

The third step was image processing, always carried out in Leica Infinity, based on SfM integrated with bundle block adjustment, using pre-calibrated camera parameters computed with an ad-hoc flight. Firstly, images were oriented, and then the DPC, DSM, and orthophoto map of the area of interest were generated, according to the following steps:

- target marking;
- image orientation and Sparse Point Cloud (SPC) generation;
- DPC generation;
- DSM generation;
- orthophoto map generation.

Figure 6 depicts a flowchart showing the steps from data collection to the generation of the deliverables.

The camera pose accuracy given in the metadata was automatically updated during the PPK, to reflect the new accuracy, and used during the photogrammetric processing, so no manual input was needed. As regards the DPC generation, to generate a clean cloud the noise reduction option was used, to remove geometrically inconsistent points in front of a reconstructed surface. Also, to ensure a complete yet accurate cloud, a sigma threshold of 0.10 m and a minimum of three images per point were chosen as dense reconstruction settings.

The geolocation precision and accuracy were checked using the 23 measured targets as both GCPs and CPs. The targets were well distributed in height (ranging from 2496.92–2675.27 m a.s.l.) and planimetry inside the area of interest as shown in Figure 1. At the end of the procedure, the DSM and orthophoto map were exported in the coordinate system used for processing (UTM system, zone 32N, EPSG: 32632), and used for the final map generation in ESRI ArcGIS Pro software.

5. Results

The DSM and orthophoto map of Forni Glacier are shown in the Main Map and bear evidence of the changes that the glacier is undergoing. The orthophoto map (left panel of the Main Map) shows the central and eastern part of the glacier tongue, separated by a medial moraine, whose elevation is about 30 m higher than the eastern tongue, as a result of differential ablation decreasing rates of ice melt

Figure 4. Equipment for data acquisition: Leica GS18 T multi-frequency GNSS receiver used as a base at the Branca hut (left), DJI Phantom 4 RTK and D-RTK 2 high-precision GNSS mobile station (center), and an example of a target (right).

under the moraine debris cover. While before the last decade only the eastern part of the moraine was fully developed (lighter brown in the left panel of the Main Map), this is now joined by a neomoraine to the west. Also, both on the central and eastern parts of the tongue are longitudinal debris septa, which might reflect debris transport from newly emerging nunataks up-valley. Collapsing areas occur at the ice margins on the central part of the tongue (bottom inset in the left panel of the Main Map), on the eastern tongue and on the medial moraines. These collapsing areas are more clearly seen on the DSM (right panel of the Main Map), as ice thinning in these areas can locally differ by more than 20 m compared to the surrounding ice surface. Water can also accumulate in the depressions, as seen on the orthophoto map on the central part of the tongue close to the terminus.

The glacier terminates abruptly on the eastern part of the medial moraine with a highly debris-covered ice cliff, while to the west the transition to the proglacial environment is more gradual (top inset in the left panel of the Main Map). The proglacial plain is also undergoing rapid changes, with continuous reworking of glaciofluvial deposits and evidence of colonisation by pioneer vegetation (greener spots in the left panel of the Main Map). The top part of the map includes the roches moutonnées, exposed by ice retreat since the 1980s, which with their striae and asymmetric slopes still bear witness to the former ice flow.

To investigate the quality of the reconstruction, GCPs, CPs, camera centres and tie points information were considered. For evaluating the precision of the image block geolocation, GCPs and camera centres were considered, while the CPs were used for the geolocation accuracy. Tables 2 and 3 show the statistical

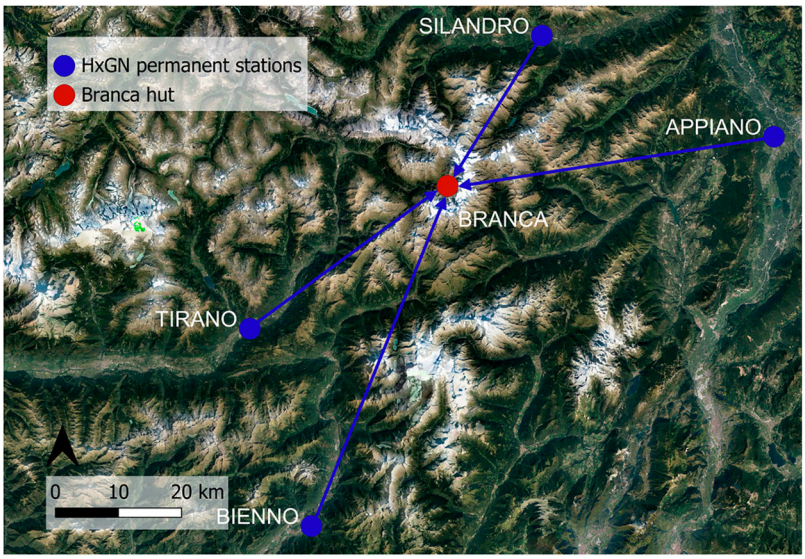

Figure 5. The location of the GNSS permanent stations used to post-process the position of the station used as base in the survey.

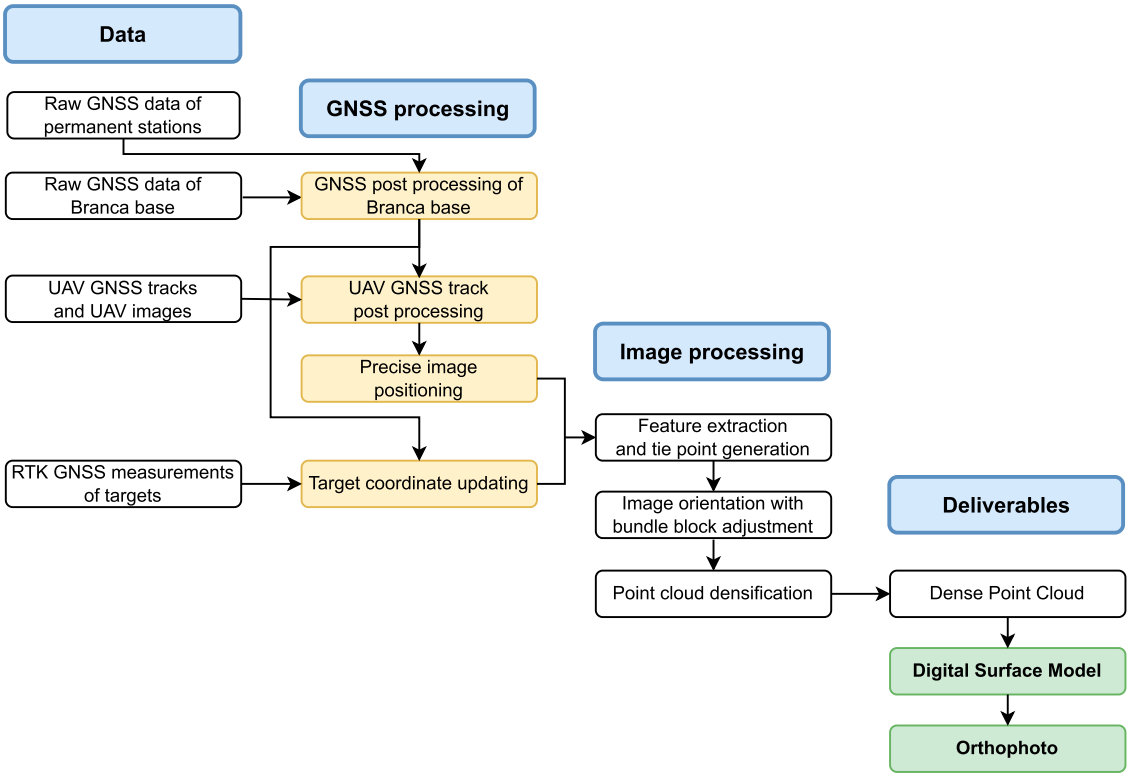

Figure 6. The flowchart of the data processing, including the GNSS data and the images to finally generate the orthophoto map and DSM.

metrics (mean, standard deviation - Std. Dev. -, and Root Mean Square Error - RMSE -) for the GCPs and the camera centres, respectively. The mean 3D residual (Δ3D) on the 15 GCPs is 4.0 cm, the Std. Dev. is 3.0 cm, the RMSE is 5.0 cm and the mean reprojection error is 1.2 px. The mean 3D residual (Δ3D) on the camera centres is 0.0 cm, the Std. Dev. is 4.0 cm, and the RMSE is 4.0 cm.

Table 4 shows the statistics on the CPs. The mean 3D residual (Δ3D) on the 8 CPs is 6.0 cm and the mean reprojection error is 1.8 px. The overall mean accuracy of the image block geolocation, represented by the RMSE of the Δ3D on CPs, is 6.0 cm.

As regards tie points, the mean number of tie points per image, affecting the density of the reconstruction, is 140, while the mean number of images where a tie point has been measured is 8 and this indicates the number of images contributing to the calculation of a 3D point and, therefore, the reliability of the result.

After the geolocation precision and accuracy of the image block were evaluated and proved suitable for the goal of this work, the DSM was exported with a GSD of 20 cm and the orthophoto map with a GSD of 3 cm, and their quality was assessed as well. The precision and accuracy of the DSM were evaluated by computing the differences between the orthometric height of the targets and the corresponding orthometric values of the DSM. The comparison was carried out for all the available targets, and then the results were aggregated separately for the GCPs and CPs, by computing five standard statistical metrics: mean, median, Std. Dev., RMSE, and Normalised Median Absolute Deviation (NMAD). The metrics are shown in Tables 5 and 6, respectively, for the GCPs and CPs.

The quite similar mean and median, and the similar Std. Dev. and NMAD highlight the absence of biases and an overall RMSE of 6 cm. For the precision and accuracy evaluation of the orthophoto map, the measured target coordinates were compared with the coordinates of the corresponding points manually marked in the orthophoto map. The 2D planimetric residual was computed for each target, and then the results of the GCPs and CPs were aggregated separately by calculating the standard statistical metrics. The results are reported in Tables 7 and 8.

Again, the similar mean and median, and the similar Std. Dev. and NMAD values highlight the absence of biases and an overall RMSE of the orthophoto map of 4 cm.

6. Discussion

The overall aim of this study was to provide up-to-date, highly accurate and detailed products of the Forni Glacier morphology, as well as setting a reference for further studies on the glacier. In this section, the factors influencing the accuracy and quality of the generated DSM and orthophoto map are first described in detail. Then, potential applications of the generated products are presented to underline

Table 2. Geolocation precision assessment with GCPs.

GCP [-]	E [m]	N [m]	Ortho. Height [m]	ΔE [m]	ΔN [m]	ΔOrtho. Height [m]	Δ3D [m]	Mean Reproj. Error [px]
22–1001	621,894.75	5,140,320.27	2,509.56	0.00	0.01	−0.09	0.09	1.3
22–1002	621,814.50	5,140,483.05	2,502.88	0.01	0.00	−0.11	0.11	1.4
22–1004	621,884.79	5,140,150.02	2,518.75	−0.01	0.00	−0.04	0.04	0.9
22–1006	622,053.55	5,139,885.55	2,549.91	0.00	0.00	−0.03	0.03	1.1
22–2048	621,893.11	5,139,831.89	2,510.02	0.00	0.01	0.01	0.02	0.4
22–2050	621,818.32	5,139,550.14	2,584.71	0.00	0.01	−0.02	0.02	1.4
22-K001	621,772.43	5,140,226.78	2,506.42	0.00	−0.01	−0.03	0.04	0.7
22-K006	621,752.74	5,140,004.88	2,516.90	0.01	0.00	0.01	0.01	0.4
22–1007	622,147.91	5,139,747.24	2,603.16	0.00	0.01	0.06	0.06	1.2
22–1008	622,222.69	5,139,562.62	2,582.09	−0.06	−0.03	0.02	0.07	2.5
22–1010	622,207.31	5,139,284.46	2,625.93	0.02	−0.03	−0.03	0.05	1.8
22–1012	622,418.88	5,139,078.78	2,675.27	0.00	0.00	−0.01	0.01	0.8
22–2003	621,881.00	5,139,361.03	2,593.15	0.00	−0.01	−0.02	0.02	0.4
22–2004	622,088.19	5,138,983.91	2,662.23	−0.01	−0.01	−0.06	0.06	2.4
22–2006	622,241.18	5,138,996.62	2,670.86	0.01	−0.01	−0.02	0.03	1.5
			Mean	**0.00**	**0.00**	**−0.02**	**0.04**	**1.2**
			Std. Dev.	**0.02**	**0.01**	**0.04**	**0.03**	**0.6**
			RMSE	**0.02**	**0.01**	**0.05**	**0.05**	**1.4**

the importance of such high-accurate and detailed deliverables for glacier monitoring.

6.1. Factors affecting the quality of the generated DSM and orthophoto map

Many are the factors influencing the accuracy and the quality of UAV photogrammetric deliverables, such as GCP density, GNSS solution, image overlap, image contrast, and light conditions (Cledat et al., 2020; Gindraux et al., 2017; Groos et al., 2022; Van Tricht et al., 2021; Zhang et al., 2022). Among these elements, the number and distribution of GCPs, the GNSS solution that can be utilised, the image contrast, and the light conditions are highly affected by environmental conditions (such as complex terrain morphologies, or snow-covered mountain areas), while the image overlap is independent of the study area (Groos et al., 2022).

The GCP density is one main factor impacting the geolocation accuracy of UAV DSMs and orthophoto maps, along with the GNSS solution type of the image coordinates. According to Gindraux et al. (2017), a density of more than 10 GCPs km^{-2} should be sufficient to generate DSMs and orthophoto maps with a decimetre accuracy (Groos et al., 2022). Similarly, Van Tricht et al. (2021) adopted a density of 10–20 GCPs km^{-2} for estimating surface mass balance patterns from UAV measurements. As widely investigated (Rangel et al., 2018; Zhang et al., 2022), besides GCP density, GCP distribution also affects the deliverable accuracy. A uniform GCP distribution in planimetry is ideal, even if this is often not feasible in mountain terrain due to inaccessible or dangerous areas. In not perfectly flat areas, GCPs should also be placed across different elevations to ensure a good constraint in height as well. In our work, we adopted 15 well-distributed GCPs over an area of 0.8 km^2 and we achieved an accuracy of a few centimetres evaluated using 8 CPs.

Table 3. Geolocation precision assessment with camera centres.

Statistics	ΔE [m]	ΔN [m]	ΔOrtho. Height [m]	Δ3D [m]
Mean	0.00	0.00	0.00	0.00
Std. Dev.	0.02	0.02	0.03	0.04
RMSE	0.02	0.02	0.03	0.04

As regards the GNSS solution, some drones can store GNSS raw data suitable for PPK workflow, ensuring the best accuracy, beneficial especially in complex natural environments (Cledat et al., 2020). They can also work with RTK positioning receiving corrections in real-time, perform an autonomous flight when not connected to any local base station, or even navigate and acquire data without GNSS. For areas where a data connection is not stable or not available, as often happens in mountain areas, and as it occurs on Forni Glacier, the PPK workflow is the best option to go for, as it ensures control in the office of the quality of the GNSS data and provides the best possible accuracy. Ground points, used as GCPs and CPs, are of crucial importance to evaluate the geolocation precision and accuracy of the results, so it is advised to use them when the physical environment allows. In this study, an approach with PPK was used to obtain the best accuracy; ground targets were also used for redundancy and geolocation accuracy evaluation.

As for image contrast, the image-matching procedure during the photogrammetric processing is usually hampered in the areas covered by fresh snow, since the low contrast reduces the number of matching tie-points and introduces some artefacts in the deliverables (Groos et al., 2022). In our study, we performed the UAV survey in the summer period (which was also the hottest summer on record in Europe) to avoid fresh snow. Also, the presence of medial moraines, and supraglacial debris cover, as well as the darkening process of the glacier surface in the study area (Azzoni et al., 2018; Fugazza et al., 2019), increased the texture of the images, facilitating the matching procedure.

Table 4. Geolocation accuracy assessment with CPs.

CP [-]	E [m]	N [m]	Ortho. Height [m]	ΔE [m]	ΔN [m]	ΔOrtho. Height [m]	Δ3D [m]	Mean Reproj. Error [px]
22–1003	621,905.23	5,140,224.39	2,516.44	0.00	0.01	−0.09	0.09	1.5
22–1005	621,933.45	5,140,045.55	2,529.15	0.00	0.00	−0.05	0.05	0.7
22–2002	621,746.43	5,139,770.84	2,546.18	0.02	0.00	−0.02	0.02	1.0
22-K003	621,699.71	5,140,308.01	2,496.92	0.00	−0.01	−0.06	0.06	0.8
22–1009	622,085.70	5,139,473.83	2,591.40	0.02	−0.01	0.04	0.05	0.7
22–1011	622,247.60	5,139,087.16	2,654.95	0.02	−0.07	−0.04	0.08	6.3
22–1013	622,431.85	5,139,383.51	2,615.93	0.02	0.01	−0.03	0.04	0.9
22–2005	622,030.04	5,139,152.79	2,633.33	0.00	−0.01	−0.08	0.08	2.2
			Mean	**0.01**	**−0.01**	**−0.04**	**0.06**	**1.8**
			Std. Dev.	**0.01**	**0.02**	**0.04**	**0.02**	**1.8**
			RMSE	**0.01**	**0.03**	**0.06**	**0.06**	**2.5**

Illumination conditions also have an impact on 3D reconstructions, especially in the mountain environment where clouds are common and the weather can change very quickly (Gaffey & Bhardwaj, 2020). In our work, the acquisition was partially affected by rolling clouds causing rapid changes in weather conditions. For this reason, the orthophoto map generated in our work has partially non-uniform lighting. In such cases, one possible solution is to wait for more stable lighting conditions; however, this was not possible during our survey due to logistic constraints.

Finally, regarding image overlap, as already highlighted, careful flight planning enables the acquisition of UAV images with sufficient lateral overlap (>70–80%) and this is essential for finding an adequate compromise between sharp image details (i.e. small GSD), complete coverage of the area of interest, and reasonable flight time (Groos et al., 2022). Rosnell and Honkavaara (2012) performed several UAV flights over the same area, using longitudinal overlap from 60% to 90%. They found that increasing the overlap clearly improves the deliverable accuracy, due to a better estimation of the image block orientation parameters and they recommended an overlap higher than 80%. Gindraux et al. (2017) set an 80% lateral and 75% longitudinal overlap between adjacent images acquired over a glacier environment. Similarly, in our study, we adopted a 75% lateral and 80% longitudinal overlap which represents a good compromise between image resolution, area coverage, and power battery consumption.

6.2. Potential applications of the generated DSM and orthophoto map

As for possible applications, the generated high-accuracy products can be used to investigate many aspects related to the glacier and its evolution, from glacier thinning to geomorphological mapping. The high accuracy of the DSM makes it suitable for comparison over timescales from seasonal to annual, allowing to infer the glacier thinning patterns during the ablation season or from year to year. As for volume change evaluation, different works can be found in the literature. Among them, Benoit et al. (2019) produced a stack of co-registered DSMs and orthophoto maps of Gorner Glacier (Switzerland) from 10 UAV surveys performed in 2017.

Besides glacier thinning, DSM differencing can also be combined with meteorological data to estimate the ablation of debris-covered ice areas (Westoby et al., 2020), such as the medial moraines of Forni glacier, or used to infer the glacier mass balance and compare the results with the direct glaciological method (ablation stakes), provided that the elevation changes are corrected for ice flux divergence (e.g. Van Tricht et al., 2021). To estimate this parameter, the calculation of ice surface velocities is required, which by itself can also inform on the dynamics of the glacier and help identify areas of stagnating ice more prone to collapse (Egli et al., 2021). Surface velocities can be measured manually (Ioli et al., 2021) or by automatic tracking of features such as crevasses and boulders (Che et al., 2020), which can be easily found on the orthophoto maps.

Again, the high accuracy of the orthophoto maps generated in this study (see Table 8) ensures a minimal impact of geolocation errors on the calculations, although the high detail can make the procedure computationally intensive for feature tracking software (Lamsters et al., 2022). The orthophoto map, alone or in combination with the DSM, also lends itself to the investigation of glacier morphologies, including supraglacial (Fugazza et al., 2015) and periglacial features (Ewertowski et al., 2019). Here, the high resolution makes it possible to document recent morphological changes of the deglaciated landscapes

Table 5. DSM vertical geolocation precision: the statistical analysis using the GCPs.

GCP	Mean	Median	Std. Dev.	RMSE	NMAD
ΔHeight [m]	−0.04	−0.06	0.06	0.07	0.06

Table 6. DSM vertical geolocation accuracy: the statistical analysis using the CPs.

CP	Mean	Median	Std. Dev.	RMSE	NMAD
ΔHeight [m]	−0.04	−0.03	0.04	0.05	0.06

Table 7. Orthophoto map geolocation precision: the statistical analysis using the GCPs.

GCP	Mean	Median	Std. Dev.	RMSE	NMAD
Δ2D [m]	0.03	0.02	0.02	0.03	0.01

with detail not feasible with other aerial imagery, and calculate their parameters (Ely et al., 2017), as well as investigate patterns of vegetation colonisation (D'Agata et al., 2020).

7. Conclusions

In this paper, we presented a high-resolution and high-accuracy orthophoto map and a DSM of Forni Glacier, generated from a UAV survey carried out in August 2022. For processing the data we combined the PPK strategy and the SfM technique, integrated with bundle block adjustment and usage of ground points, to achieve the best possible result by improving the accuracy of the final deliverables. We carried out the whole processing pipeline in Leica Infinity and we evaluated the geolocation precision and accuracy of the processing using 15 GCPs and 8 CPs over an area of 0.8 km^2. We achieved an overall mean 3D geolocation accuracy of the image block of 6.0 cm, as computed on the CPs. Then, we evaluated the geolocation precision and accuracy of the final deliverables by computing the differences between the measured target coordinates and the corresponding target positions on the orthophoto map and DSM. We generated a 3 cm GSD orthophoto map and a 20 cm GSD DSM that showed uncertainties in RMSE (NMAD) of 0.04 m (0.02 m) and 0.05 m (0.06 m) considering 2D and 3D geolocation accuracy, respectively. We also prepared a map with the generated products which is available as an attachment to the paper. The generated products provide up-to-date accurate and high-resolution data that can be used as a reference for future investigations of this glacier, analysing the impact of climate change on its evolution, such as information on the glacier thinning and surface velocity patterns, which also allows estimating the glacier mass balance and generating highly detailed mapping of glacier morphologies.

Software

The areas for the flights were designed and created in Leica Infinity 4.0. The flights were planned and flown with the Phantom 4 RTK Remote Controller V2.1.2. Post-processing of GNSS measurements and image processing for the DSM and orthophoto map generation were done using Leica Infinity 4.0. The final map with the orthophoto map and DSM was generated using ESRI ArcGIS Pro 3.0.2.

Table 8. Orthophoto map geolocation accuracy: the statistical analysis using the CPs.

CP	Mean	Median	Std. Dev.	RMSE	NMAD
Δ2D [m]	0.04	0.03	0.02	0.04	0.02

Acknowledgments

The authors would like to thank the Stelvio Park Authority for permitting the UAV surveys and the Branca hut for the logistic support. The authors are also thankful to Federica Leotta, Francesco Maini, Flavia Marini and Sara Bonomelli for their help during the survey.

Disclosure statement

No potential conflict of interest was reported by the authors.

Funding

The present study was partially supported by Levissima Sanpellegrino S.P.A. through an agreement with UNIMI, grant number LIB_17VTGDIOL and a Post-Doc grant at Sapienza University of Rome.

Data availability statement

The orthophoto map and DSM of Forni Glacier are available in the supplementary materials of this paper.

ORCID

Valeria Belloni http://orcid.org/0000-0003-4765-0281
Martina Di Rita http://orcid.org/0000-0001-9670-1167
Davide Fugazza http://orcid.org/0000-0003-4523-9085
Giacomo Traversa http://orcid.org/0000-0003-3108-887X
Guglielmina Diolaiuti http://orcid.org/0000-0002-3883-9309
Mattia Crespi http://orcid.org/0000-0002-0592-6182

References

Azzoni, R. S., Fugazza, D., Zennaro, M., Zucali, M., D'Agata, C., Maragno, D., Cernuschi, M., Smiraglia, C., & Diolaiuti, G. A. (2017). Recent structural evolution of Forni Glacier tongue (Ortles-Cevedale Group, Central Italian Alps). *Journal of Maps*, *13*, 870–878. https://doi.org/10.1080/17445647.2017.1394227

Azzoni, R. S., Fugazza, D., Zerboni, A., Senese, A., D'Agata, C., Maragno, D., Carzaniga, A., Cernuschi, M., & Diolaiuti, G. A. (2018). Evaluating high-resolution remote sensing data for reconstructing the recent evolution of supra glacial debris: A study in the Central Alps (Stelvio Park, Italy). *Progress in Physical Geography: Earth and Environment*, *42*, 3–23. https://doi.org/10.1177/0309133317749434

Belloni, V., Fugazza, D., & Di Rita, M. (2022, June 6–11). *UAV-based glacier monitoring: GNSS kinematic track post-processing and direct georeferencing for accurate reconstructions in challenging environments.* The International Archives of the Photogrammetry, Remote Sensing and Spatial Information Sciences. Presented at the XXIV ISPRS Congress "Imaging today, foreseeing

tomorrow", Commission I - 2022 edition, Nice, France. Copernicus GmbH (pp. 367–373). https://doi.org/10.5194/isprs-archives-XLIII-B1-2022-367-2022

Benoit, L., Gourdon, A., Vallat, R., Irarrazaval, I., Gravey, M., Lehmann, B., Prasicek, G., Gräff, D., Herman, F., & Mariethoz, G. (2019). A high-resolution image time series of the Gorner Glacier – Swiss Alps – derived from repeated unmanned aerial vehicle surveys. *Earth System Science Data*, *11*, 579–588. https://doi.org/10.5194/essd-11-579-2019

Blasone, G., Cavalli, M., & Cazorzi, F. (2015). Debris-Flow monitoring and geomorphic change detection combining laser scanning and fast photogrammetric surveys in the moscardo catchment (eastern Italian Alps). In G. Lollino, M. Arattano, M. Rinaldi, O. Giustolisi, J.-C. Marechal, & G. E. Grant (Eds.), *Engineering geology for society and territory - volume 3* (pp. 51–54). Springer International Publishing. https://doi.org/10.1007/978-3-319-09054-2_10

Che, Y., Wang, S., Yi, S., Wei, Y., & Cai, Y. (2020). Summer mass balance and surface velocity derived by unmanned aerial vehicle on debris-covered region of baishui river glacier No. 1, yulong snow mountain. *Remote Sensing*, *12*, 3280–3294. https://doi.org/10.3390/rs12203280

Cledat, E., Jospin, L. V., Cucci, D. A., & Skaloud, J. (2020). Mapping quality prediction for RTK/PPK-equipped micro-drones operating in complex natural environment. *ISPRS Journal of Photogrammetry and Remote Sensing*, *167*, 24–38. https://doi.org/10.1016/j.isprsjprs.2020.05.015

D'Agata, C., Diolaiuti, G., Maragno, D., Smiraglia, C., & Pelfini, M. (2020). Climate change effects on landscape and environment in glacierized alpine areas: Retreating glaciers and enlarging forelands in the bernina group (Italy) in the period 1954–2007. *Geology, Ecology, and Landscapes*, *4*, 71–86. https://doi.org/10.1080/24749508.2019.1585658

Dall'Asta, E., Forlani, G., Roncella, R., Santise, M., Diotri, F., & Morra di Cella, U. (2017). Unmanned aerial systems and DSM matching for rock glacier monitoring. *ISPRS Journal of Photogrammetry and Remote Sensing, Geospatial Week 2015*, *127*, 102–114. https://doi.org/10.1016/j.isprsjprs.2016.10.003

Di Mauro, B., & Fugazza, D. (2022). Pan-Alpine glacierx phenology reveals lowering albedo and increase in ablation season length. *Remote Sensing of Environment*, *279*, 113119–113133. https://doi.org/10.1016/j.rse.2022.113119

Di Rita, M., Fugazza, D., Belloni, V., Diolaiuti, G., Scaioni, M., & Crespi, M. (2020, 31 August–2 September). *Glacier volume change monitoring from UAV observations: Issues and potentials of state-of-the-art techniques*. ISPRS - International Archives of the Photogrammetry, Remote Sensing and Spatial Information Sciences. Presented at the XXIV ISPRS Congress, Commission II (Volume XLIII-B2-2020) - 2020 edition. Copernicus GmbH (pp. 1041–1048). Nice, France. https://doi.org/10.5194/isprs-archives-XLIII-B2-2020-1041-2020

Di Rita, M., & Hanson, K. (2022, June 6–11). *Data fusion for construction monitoring: How leica infinity manages images, GNSS data, terrestrial scans and BIM data to efficiently track complex construction sites*. The International Archives of the Photogrammetry, Remote Sensing and Spatial Information Sciences. Presented at the XXIV ISPRS Congress "Imaging today, foreseeing tomorrow", Commission II - 2022 edition, Nice, France. Copernicus GmbH (pp. 373–378). https://doi.org/10.5194/isprs-archives-XLIII-B2-2022-373-2022.

Egli, P. E., Belotti, B., Ouvry, B., Irving, J., & Lane, S. N. (2021). Subglacial channels, climate warming, and increasing frequency of Alpine glacier snout collapse. *Geophysical Research Letters*, *48*, 1–15. https://doi.org/10.1029/2021GL096031.

Ely, J. C., Graham, C., Barr, I. D., Rea, B. R., Spagnolo, M., & Evans, J. (2017). Using UAV acquired photography and structure from motion techniques for studying glacier landforms: Application to the glacial flutes at isfallsglaciären. *Earth Surface Processes and Landforms*, *42*, 877–888. https://doi.org/10.1002/esp.4044

Ewertowski, M. W., Tomczyk, A. M., Evans, D. J. A., Roberts, D. H., & Ewertowski, W. (2019). Operational framework for rapid, very-high resolution mapping of glacial geomorphology using low-cost unmanned aerial vehicles and structure-from-motion approach. *Remote Sensing*, *11*, 65–82. https://doi.org/10.3390/rs11010065

Fugazza, D., Scaioni, M., Corti, M., D'Agata, C., Azzoni, R. S., Cernuschi, M., Smiraglia, C., & Diolaiuti, G. A. (2018). Combination of UAV and terrestrial photogrammetry to assess rapid glacier evolution and map glacier hazards. *Natural Hazards and Earth System Sciences*, *18*, 1055–1071. https://doi.org/10.5194/nhess-18-1055-2018

Fugazza, D., Senese, A., Azzoni, R. S., Maugeri, M., & Diolaiuti, G. A. (2016). Spatial distribution of surface albedo at the Forni Glacier (Stelvio National Park, Central Italian Alps). *Cold Regions Science and Technology*, *125*, 128–137. https://doi.org/10.1016/j.coldregions.2016.02.006

Fugazza, D., Senese, A., Azzoni, R. S., Maugeri, M., Maragno, D., & Diolaiuti, G. A. (2019). New evidence of glacier darkening in the Ortles-Cevedale group from Landsat observations. *Global and Planetary Change*, *178*, 35–45. https://doi.org/10.1016/j.gloplacha.2019.04.014

Fugazza, D., Senese, A., Azzoni, R. S., Smiraglia, C., Cernuschi, M., Severi, D., & Diolaiuti, G. A. (2015). High-resolution mapping of glacier surface features. The UAV survey of the Forni glacier (Stelvio National Park, Italy). *Geografia Fisica e Dinamica Quaternaria*, *38*, 25–33. https://doi.org/10.4461/GFDQ.2015.38.03

Gaffey, C., & Bhardwaj, A. (2020). Applications of unmanned aerial vehicles in cryosphere: Latest advances and prospects. *Remote Sensing*, *12*, 948–987. https://doi.org/10.3390/rs12060948

Gindraux, S., Boesch, R., & Farinotti, D. (2017). Accuracy assessment of digital surface models from unmanned aerial vehicles' imagery on glaciers. *Remote Sensing*, *9*, 186–200. https://doi.org/10.3390/rs9020186

Groos, A. R., Aeschbacher, R., Fischer, M., Kohler, N., Mayer, C., & Senn-Rist, A. (2022). Accuracy of UAV photogrammetry in glacial and periglacial alpine terrain: a comparison with airborne and terrestrial datasets. *Frontiers in Remote Sensing*, *3*, 1–16. https://doi.org/10.3389/frsen.2022.871994

Ioli, F., Bianchi, A., Cina, A., De Michele, C., Maschio, P., Passoni, D., & Pinto, L. (2021). Mid-term monitoring of glacier's variations with UAVs: the example of the belvedere glacier. *Remote Sensing*, *14*, 28–46. https://doi.org/10.3390/rs14010028

Lamsters, K., Ješkins, J., Sobota, I., Karušs, J., & Džeriņš, P. (2022). Surface characteristics, elevation change, and velocity of high-arctic valley glacier from repeated high-resolution UAV photogrammetry. *Remote Sensing*, *14*, 1029–1048. https://doi.org/10.3390/rs14041029

Maier, K., Nascetti, A., van Pelt, W., & Rosqvist, G. (2022). Direct photogrammetry with multispectral imagery for UAV-based snow depth estimation. *ISPRS Journal of Photogrammetry and Remote Sensing*, *186*, 1–18. https://doi.org/10.1016/j.isprsjprs.2022.01.020

Paul, F., Rastner, P., Azzoni, R. S., Diolaiuti, G., Fugazza, D., Le Bris, R., Nemec, J., Rabatel, A., Ramusovic, M., Schwaizer, G., & Smiraglia, C. (2020). Glacier shrinkage in the Alps continues unabated as revealed by a new glacier inventory from Sentinel-2. *Earth System Science Data*, *12*, 1805–1821. https://doi.org/10.5194/essd-12-1805-2020

Rangel, J. M. G., Gonçalves, G. R., & Pérez, J. A. (2018). The impact of number and spatial distribution of GCPs on the positional accuracy of geospatial products derived from low-cost UASs. *International Journal of Remote Sensing*, *39*, 7154–7171. https://doi.org/10.1080/01431161.2018.1515508

Rosnell, T., & Honkavaara, E. (2012). Point cloud generation from aerial image data acquired by a quadrocopter type micro unmanned aerial vehicle and a digital still camera. *Sensors (Basel)*, *12*, 453–480. https://doi.org/10.3390/s120100453

Rossini, M., Di Mauro, B., Garzonio, R., Baccolo, G., Cavallini, G., Mattavelli, M., De Amicis, M., & Colombo, R. (2018). Rapid melting dynamics of an alpine glacier with repeated UAV photogrammetry. *Geomorphology*, *304*, 159–172. https://doi.org/10.1016/j.geomorph.2017.12.039

Senese, A., Diolaiuti, G., Mihalcea, C., & Smiraglia, C. (2012). Energy and mass balance of Forni Glacier (Stelvio National Park, Italian Alps) from a four-year meteorological data record. *Arctic, Antarctic, and Alpine Research*, *44*, 122–134. https://doi.org/10.1657/1938-4246-44.1.122

Senese, A., Maugeri, M., Meraldi, E., Verza, G. P., Azzoni, R. S., Compostella, C., & Diolaiuti, G. (2018). Estimating the snow water equivalent on a glacierized high elevation site (Forni Glacier, Italy). *The Cryosphere*, *12*, 1293–1306. https://doi.org/10.5194/tc-12-1293-2018

Smiraglia, C., Azzoni, R. S., D'Agata, C., Maragno, D., Fugazza, D., & Diolaiuti, G. A. (2015). The evolution of the Italian glaciers from the previous data base to the new Italian inventory. Preliminary considerations and results. *Geografia Fisica e Dinamica Quaternaria*, *38*, 79–87. https://doi.org/10.4461/GFDQ.2015.38.08

Urbini, S., Zirizzotti, A., Baskaradas, J., Tabacco, I. E., Cafarella, L., Senese, A., Smiraglia, C., & Diolaiuti, G. (2017). Airborne Radio Echo Sounding (RES) measures on Alpine Glaciers to evaluate ice thickness and bedrock geometry: preliminary results from pilot tests performed in the Ortles Cevedale Group (Italian Alps). *Annals of Geophysics*, *60*, G0226–G0226. https://doi.org/10.4401/ag-7122

Van Tricht, L., Huybrechts, P., Van Breedam, J., Vanhulle, A., Van Oost, K., & Zekollari, H. (2021). Estimating surface mass balance patterns from unoccupied aerial vehicle measurements in the ablation area of the morteratsch–pers glacier complex (Switzerland). *The Cryosphere*, *15*, 4445–4464. https://doi.org/10.5194/tc-15-4445-2021

Westoby, M. J., Rounce, D. R., Shaw, T. E., Fyffe, C. L., Moore, P. L., Stewart, R. L., & Brock, B. W. (2020). Geomorphological evolution of a debris-covered glacier surface. *Earth Surface Processes and Landforms*, *45*, 3431–3448. https://doi.org/10.1002/esp.4973

WGMS. (2021). *Global glacier change bulletin No. 4 (2018-2019)*. ISC (WDS), IUGG (IACS), UNEP, UNESCO, WMO.

Zemp, M., Huss, M., Thibert, E., Eckert, N., McNabb, R., Huber, J., Barandun, M., Machguth, H., Nussbaumer, S. U., Gärtner-Roer, I., Thomson, L., Paul, F., Maussion, F., Kutuzov, S., & Cogley, J. G. (2019). Global glacier mass changes and their contributions to sea-level rise from 1961 to 2016. *Nature*, *568*, 382–386. https://doi.org/10.1038/s41586-019-1071-0

Zhang, K., Okazawa, H., Hayashi, K., Hayashi, T., Fiwa, L., & Maskey, S. (2022). Optimization of ground control point distribution for unmanned aerial vehicle photogrammetry for inaccessible fields. *Sustainability*, *14*, 9505–9525. https://doi.org/10.3390/su14159505